

Poromechanical response of fractured-porous rock masses

Mao Bai ^{a,*}, Jean-Claude Roegiers ^a, Derek Elsworth ^b

^a School of Petroleum and Geological Engineering, University of Oklahoma, Norman, OK 73019-0628, USA

^b Department of Mineral Engineering, Pennsylvania State University, University Park, PA, USA

Received 19 April 1994; accepted 2 May 1995

Abstract

An analytical model based on a poromechanical formulation for dual-porosity media is presented. In comparison with traditional conceptualizations such as by Barenblatt et al. (1960), the proposed model contains both additional terms in the governing flow equations to provide a physically more realistic description of the change in storage, and a natural accommodation of body displacements. Solution is developed for radial flow in a reservoir subject to the conditions of both constant bottom hole pressure and constant flow rate using Hankel transforms. The poromechanical effect, resulting from the coupling between fluid flow and solid deformation, is significant in the well vicinity where the modifications of initial pressure and stress state are substantial. Different from the conventional approach in which the impact of fluid properties is generally emphasized, the presented case studies highlight the critical influence of mechanical properties of the fractured rock mass on the change of fluid pressure in a producing reservoir. The study indicates that dual-porosity behavior is most obvious only when the poromechanical properties fall within a certain range.

1. Introduction

The behavior of fractured porous rock masses is different from unfractured-porous media because of their unique flow characteristics along with unique mechanical responses to the internally and externally applied loads. Porous rock masses are deposited as sediments of matrix rock with intergranular porosity. Over geological time, continuity of these masses has been disrupted as a result of tectonic activities, weathering, earthquakes, glacial and thermal stresses. The resulting rock masses may be described as aggregates of blocks bounded by interconnected or isolated fractures, adding secondary porosity to the original porous materials. In general, the fluid flow within matrix blocks is different from the flow in a fractured network. In the former, the matrix blocks contain pore space having similar dimen-

sions in lengths and widths, in addition to highly tortuous flow patterns. In the latter, the fractures provide more continuous apertures with lengths far in excess of their widths. If several closely spaced sets of joints are present, they may form a directly interconnected flow system. The combination of radial intergranular flow in the matrix blocks with linear flow in fractures represents a typical flow pattern within naturally-fractured reservoirs.

In general, conservation laws hold for momentum, mass and energy. For an isothermal case, stress equilibrium must be maintained for the load-deformation behavior of the reservoir, while fluid mass is concurrently conserved. Reservoir deformation as a result of production is coupled with induced pore pressure change. This effect is most pronounced in areas of large changes in total stress, such as in the vicinity of pro-

* Corresponding author.

ducing wells, with the magnitude of this impact diminishing with distance.

Analytical solutions for flow in deformation-coupled dual porosity systems provide an important means of distilling the essential behavioral components in the response, albeit for simplified geometric representations of reality. The governing equations representing flow through fractured-porous media were initially proposed by Barenblatt et al. (1960). The mathematical model was further developed as a potential reservoir simulator by Warren and Root (1963). Analytical solutions for flow towards a single well are available for a variety of reservoir conditions. Streltsova-Adams (1978) evaluated many of the possible solutions based on the dual-porosity conceptualization. Raghavan (1977) proposed several approaches for wells intercepting single discrete fractures. Moench (1984) assumed an interactive dual-porosity behavior as that fluid flows across a fracture skin. In terms of coupling fluid flow with solid deformation, Biot (1941) presented a comprehensive poroelastic formulation in three-dimensional space, with displacement and pressure as primary unknowns. Rice and Cleary (1976) introduced a series of alternative solutions based on the stress function method and provided a unification between the theory of Biot and that developed by Terzaghi (1923). Using the solution of Melan (1940) for a central point dilatation in a semi-elastic space, Segall (1985) solved the coupled flow-deformation problem for a reservoir subjected to fluid extraction. Recent advances extend the traditional dual-porosity approach to encompass the coupled processes which include partial or comprehensive coupling of fluid flow, solid deformation, heat transfer and solute transport (Bai et al., 1993; Bai and Roegiers, 1995). Research efforts have also been focused on identifying local influences such as convective flow (Bai and Roegiers, 1994) or nonlinear flow near a well (Bai et al., 1994) in a dual-porosity medium. Accompanying numerical advances include the development of a three-dimensional finite-element model capable of evaluating coupled flow-deformation in poroelastic dual-porosity media (Bai and Meng, 1994).

This paper presents an alternative dual-porosity model based on a modification of Barenblatt et al.'s formulation (1990) and additionally incorporating full coupling of displacements. The addition of terms in the governing flow equations provides a more realistic rep-

resentation of the fluid storage interaction between matrix blocks and fractures during the initial transient flow regime. The states of stress and deformation near a producing well have been examined via a poromechanical coupling. The solutions of the constant bottom hole pressure for an infinite reservoir and the constant flow rate for a finite reservoir are obtained using Hankel transforms. A hypothetical case study focuses on the constant flow rate scenario, in an attempt to identify the dual-porosity behavior of the fractured-porous rock mass in conjunction with its poromechanical effect along with the variation of the material properties.

2. Theoretical formulation

In the dual-porosity poromechanical formulation, the governing equations for the solid and fluid phases can be written as (Wilson and Aifantis, 1982):

$$Gu_{i,jj} + (\lambda + G)u_{k,ki} + \sum_{m=1}^2 \phi_m p_{m,i} = 0 \quad (1)$$

$$\frac{k_m}{\mu} p_{m,kk} + \phi_m \dot{\epsilon}_{kk} - \phi_m^* \dot{p}_m \pm \Gamma(\Delta p) = 0 \quad (2)$$

where $m = 1$ and 2 , represent the matrix and fractures, respectively; λ and G are the Lamé constants, ϕ is the fluid pressure ratio factor or Biot coefficient (Biot, 1941), ϕ^* is the relative compressibility representing the lumped deformability of the fluid and the fractured or intact medium, k is the permeability, μ is the fluid dynamic viscosity, Γ is the transfer coefficient, u is the solid displacement, p is the fluid pressure, ϵ_{kk} is the total body strain, Δp is the pressure difference between fractures and matrix blocks. A sign convention, assuming fluid compression as positive and tension in solid stress as negative, is adopted, consistent with the field of geomechanics. The stress-strain relationship in a poroelastic medium may be expressed as:

$$\sigma_{ij} = 2G\epsilon_{ij} + \delta_{ij}\lambda\epsilon_{kk} + \delta_{ij}\sum_{m=1}^2 \phi_m p_m \quad (3)$$

The complete analogy between poroelasticity and thermoelasticity was first identified by Biot (1956). As pointed out by Rice and Cleary (1976) the analogy holds only when the coupling between the fluid pressure (or temperature) and stresses is rigorously

retained. In other words, the pressure should be derived from the governing equations simultaneously with either stresses or temperature (Cleary, 1977). In poroelasticity, complete decoupling may cause a significant error, however, only in close proximity to the application of load (Cryer, 1962). In an infinite medium, partial decoupling using the concept of displacement potential offers an acceptable approximation to that of rigorous coupling, even adjacent to a fluid source (Curran and Carvalho, 1987). As a result, a simple sequential solution procedure is then permissible. For an infinite medium with isotropic and homogeneous properties, the solid displacement can be expressed in terms of a displacement potential proposed by Goodier (1936), assuming the displacement field is irrotational as:

$$u_i = \Phi_{,i} \quad (4)$$

Substituting Eq. 4 into Eq. 1, gives:

$$G\Phi_{,ikk} + (\lambda + G)\Phi_{,kki} + \sum_{m=1}^2 \phi_m p_{m,i} = 0 \quad (5)$$

Integrating Eq. 5 with respect to x_i , results in a Poisson equation:

$$\Phi_{,kk} = \epsilon_{kk} = -\beta \sum_{m=1}^2 \phi_m p_m \quad (6)$$

where:

$$\beta = \frac{1}{2G + \lambda} = \frac{(1 + \nu)(1 - 2\nu)}{E(1 - \nu)} \quad (7)$$

where E is the elastic modulus, ν is the Poisson's ratio. Substituting Eq. 6 into Eq. 2, yields:

$$\frac{k_m}{\mu} p_{m,kk} - \beta \phi_m \sum_{m=1}^2 \phi_m \dot{p}_m - \phi_m \dot{p}_m \pm \Gamma(\Delta p) = 0$$

In a dual-porosity medium, if the rate change of fluid accumulation in the control volume is a result of exchange in storage capacity in the matrix and fractures, in addition to the volume exchange due to fluid flow between fractures and matrix blocks, then the flow equation should be further modified, in a long form, as:

$$\begin{cases} \frac{k_1}{\mu} p_{1,kk} = (\beta \phi_1^* + \phi_1^*) \dot{p}_1 - (\phi_2^* - \beta \phi_1 \phi_2) \dot{p}_2 + \Gamma(p_1 - p_2) \\ \frac{k_2}{\mu} p_{2,kk} = (\beta \phi_2^* + \phi_2^*) \dot{p}_2 - (\phi_1^* - \beta \phi_1 \phi_2) \dot{p}_1 - \Gamma(p_1 - p_2) \end{cases} \quad (8)$$

Expressing the relative compressibilities in a more explicit form, and neglecting the influence of shear-induced dilation of the fractures, Eq. 8 can be written for the matrix and the fractures, respectively:

$$\frac{k_1}{\mu} \nabla^2 p_1 = f_1 \frac{\partial p_1}{\partial t} - f_2 \frac{\partial p_2}{\partial t} + \Gamma(p_1 - p_2) \quad (9)$$

$$\frac{k_2}{\mu} \nabla^2 p_2 = f_3 \frac{\partial p_2}{\partial t} - f_4 \frac{\partial p_1}{\partial t} - \Gamma(p_1 - p_2) \quad (10)$$

where f_1 and f_3 are the matrix and fracture compressibilities, f_2 and f_4 are the interacting bulk compressibilities of the fracture and matrix phases, respectively. More explicitly:

$$f_1 = \frac{1 - n_1}{K_s} + \frac{n_1}{K_f} + \phi_1^2 \beta \quad (11)$$

$$f_2 = \frac{2n_2^*}{K_n s^* + K_f} - \phi_1 \phi_2 \beta \quad (12)$$

$$f_3 = \frac{1 - n_2}{K_n s^*} + \frac{n_2}{K_f} + \phi_2^2 \beta \quad (13)$$

$$f_4 = \frac{2n_1^*}{K_s + K_f} - \phi_1 \phi_2 \beta \quad (14)$$

where n_1 and n_2 are the porosities for matrix and fractures, respectively; K_s and K_f are the bulk moduli of solid grains and fluid, respectively; K_n is the normal fracture stiffness, s^* is the fracture spacing, n_1^* and n_2^* are the effective porosities in matrix and in fractures considering an average bulk compressibility in matrix and in fractures containing fluids, respectively. It is important to note that the governing Eqs. 9 and 10, for fluid flow alone, are different from those proposed by Barenblatt et al. (1990). Barenblatt et al. assumed that the change of the guest fluid pressure (here meant for fracture pressure in matrix flow equation, and vice versa) should have an impact on the change of void space in the host phase and this impact was omitted in their final formulation. It is arguable, however, that the storage change in the host phase (e.g. matrix) due to fluid and solid compressibilities in the guest phase (e.g. fractures) should occur in its own space. The storage change in the guest phase may contribute substantially to the change of fluid volume in the host phase, particularly in the initial transient pumping stage. This proposition may be further clarified as follows.

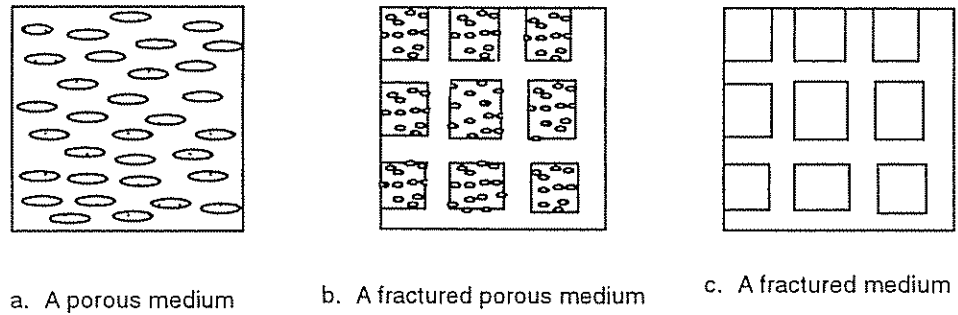


Fig. 1. Schematic fractured/porous media.

In the absence of fractures (Fig. 1a), fluid flow can be represented by:

$$\frac{k_1}{\mu} \nabla^2 p_1 = f_1 \frac{\partial p_1}{\partial t} \quad (15)$$

As a result of the presence of fractures, as shown in Fig. 1b, the fluid compressibility due to pressure change in the fracture space would counteract the rate change of fluid accumulation in the matrix space (second term on the right-hand side of Eq. 9), while the internal fluid flow due to pressure difference between matrix and fractures would either assist or counteract the matrix fluid accumulation, depending on the magnitude of pressure p_1 and p_2 (third term on the right-hand side of Eq. 9). Eq. 9 results.

Similarly, fluid flow in a fractured medium, intercepted by the impermeable matrix blocks (Fig. 1c), may be represented by:

$$\frac{k_2}{\mu} \nabla^2 p_2 = f_3 \frac{\partial p_2}{\partial t} \quad (16)$$

Following the previous reasoning, Eq. 10 may be developed if the matrix blocks in Fig. 1c are permeable, such as in Fig. 1b, and flow between the matrix and fracture is then permitted.

To represent a long producing well zone, stress and pressure changes are assumed plane radially symmetric and, therefore, independent of the circumferential and vertical orientations. Strains are, therefore, given as:

$$\begin{cases} \epsilon_{rr} = \frac{\partial u}{\partial r} \\ \epsilon_{\theta\theta} = \frac{u}{r} \\ \epsilon_{r\theta} = \epsilon_{zz} = 0 \end{cases} \quad (17)$$

The total strain is then:

$$\Phi_{,kk} = \epsilon_{kk} = \epsilon_{rr} + \epsilon_{\theta\theta} = \frac{\partial u}{\partial r} + \frac{u}{r} \quad (18)$$

and stresses can be evaluated from Eq. 3 as:

$$\sigma_{rr} = 2G\epsilon_{rr} + \lambda\epsilon_{kk} + \sum_{m=1}^2 \phi_m p_m \quad (19)$$

$$= \beta^{-1} \frac{\partial u}{\partial r} + \lambda \frac{u}{r} + \sum_{m=1}^2 \phi_m p_m$$

$$\sigma_{\theta\theta} = 2G\epsilon_{\theta\theta} + \lambda\epsilon_{kk} + \sum_{m=1}^2 \phi_m p_m \quad (20)$$

$$= \beta^{-1} \frac{u}{r} + \lambda \frac{\partial u}{\partial r} + \sum_{m=1}^2 \phi_m p_m$$

and:

$$\sigma_{zz} = \nu(\sigma_{rr} + \sigma_{\theta\theta}) = \lambda\epsilon_{kk} + 2\nu \sum_{m=1}^2 \phi_m p_m \quad (21)$$

In a radial system, Eq. 1 can be reformulated as:

$$\beta^{-1} \frac{\partial}{\partial r} \left[\frac{1}{r} \frac{\partial}{\partial r} (ru) \right] + \sum_{m=1}^2 \phi_m \frac{\partial p_m}{\partial r} = 0 \quad (22)$$

Integrating Eq. 22 with respect to r , and assuming $r \rightarrow \infty$, Δu and $\Delta p_m \rightarrow 0$ (Δ indicates the change over initial values), yields:

$$\frac{\partial u}{\partial r} + \frac{u}{r} = -\beta \sum_{m=1}^2 \phi_m p_m \quad (23)$$

Note that Eq. 23 is identical to the combination of Eqs. 6 and 18.

The solution is more general if it is solved in a dimensionless form. Therefore, we introduce the following parameters:

Dimensionless fluid pressure:

$$P_{Di} = \frac{2\pi h(k_1 + k_2)(p_0 - p_i)}{q\mu} \quad (i = 1, 2) \quad (24)$$

where h is the reservoir thickness, p_0 is the initial fluid pressure, q is the flow rate.

Dimensionless radial distance:

$$r_D = \frac{r}{r_w} \quad (25)$$

where r_w is the well radius.

Dimensionless time:

$$t_D = \frac{(k_1 + k_2)t}{\mu r_w^2 \sum_{i=1}^4 f_i} \quad (26)$$

Dimensionless displacement:

$$U_D = \frac{u_0 - u}{r_w} \quad (27)$$

where u_0 is the initial displacement.

Fluid transfer coefficient:

$$\lambda^* = \frac{\Gamma r_w^2 \mu}{k_1} = \alpha^* r_w^2 \quad (28)$$

where α^* is a shape factor (Warren and Root, 1963) and can be evaluated by the equation:

$$\alpha^* = \frac{4j^*(j^* + 2)}{\zeta^2}$$

where $j^* = 1, 2$ or 3 in terms of the number of orthogonal sets of fractures, ζ is a characteristic dimension of the blocks, and can be written as:

$$\zeta = \frac{3a^*b^*c^*}{a^*b^* + b^*c^* + c^*a^*}$$

For the regularly spaced parallelepiped model, $j^* = 3$, $a^* = b^* = c^* = s^*$; so that

$$\alpha^* = \frac{60}{(s^*)^2}$$

Elastic coefficient:

$$\beta^* = \beta \frac{q\mu}{2\pi h(k_1 + k_2)} \quad (29)$$

Calculating coefficients:

$$\omega_i = \frac{(k_1 + k_2)f_i}{k_j \sum_{i=1}^4 f_i} \quad (i = 1, 2, 3, 4) \quad (30)$$

where:

$$k_j = \begin{cases} k_1 & \text{when } i = 1 \text{ and } 2 \\ k_2 & \text{when } i = 3 \text{ and } 4 \end{cases}$$

Using simple arithmetic manipulation, coefficients ω_i can be represented by dimensionless terms such as the permeability ratio k_1/k_2 , compressibility ratios $K_f/K_n s^*$, K_f/K_s , and K_f/E , along with n_i , ν and ϕ_i .

The governing Eqs. 23, 9 and 10 can be rewritten in the dimensionless form:

$$\frac{\partial U_D}{\partial r_D} + \frac{U_D}{r_D} = -\beta^* (\phi_1 P_{D1} + \phi_2 P_{D2}) \quad (31)$$

$$\frac{\partial^2 P_{D1}}{\partial r_D^2} + \frac{1}{r_D} \frac{\partial P_{D1}}{\partial r_D} = \omega_1 \frac{\partial P_{D1}}{\partial t_D} - \omega_2 \frac{\partial P_{D2}}{\partial t_D} + \lambda^* (P_{D1} - P_{D2}) \quad (32)$$

$$\frac{\partial^2 P_{D2}}{\partial r_D^2} + \frac{1}{r_D} \frac{\partial P_{D2}}{\partial r_D} = \omega_3 \frac{\partial P_{D1}}{\partial t_D} - \omega_4 \frac{\partial P_{D2}}{\partial t_D} - \lambda^* R_k (P_{D1} - P_{D2}) \quad (33)$$

Solutions and solution procedures of solving simultaneous Eqs. 31, 32 and 33 for the cases of constant bottom-hole pressure and constant pumping rate are described in Appendices A and B, respectively.

3. Parametric relationships

The parameters used in the previous formulation for the fractured-porous rock mass may be classified into four categories, as: (a) fluid properties (K_f , μ); (b) mechanical properties (E , ν , K_n , K_s); (c) physical properties (s^* , k_1 , k_2 , n_1 , n_2 , Γ); (d) and poromechanical properties (ϕ_1 , ϕ_2). Most fluid and mechanical parameters can be routinely obtained through labora-

Table 1
Referenced material properties

| Parameter | Symbol | Value | Unit | Type | Reference |
|-----------------------|----------|--------------------------|-----------------|----------------------|-------------------------|
| Elastic modulus | E | 5 ~ 80 | GPa | sandstone | Jumikis, 1983 |
| Poisson ratio | ν | 0.07 ~ 0.33 | | sandstone, limestone | Jumikis, 1983 |
| Fluid bulk modulus | K_f | 0.5 ~ 5 | GPa | oil | Craft and Hawkins, 1959 |
| | | 3.3 | GPa | water | Rice and Cleary, 1976 |
| Grain bulk modulus | K_g | 36 ~ 50 | GPa | sandstone, marble | Rice and Cleary, 1976 |
| Fracture stiffness | K_n | 0.1 | GPa/cm | | Iwai, 1976; Rosso, 1976 |
| Fracture spacing | s^* | 0.2 ~ 30 | m | | Snow, 1968 |
| Matrix porosity | n_1 | 0.04 ~ 0.2 | | sandstone, limestone | Jumikis, 1983 |
| Fracture porosity | n_2 | 0.0001 ~ 0.01 | | | Snow, 1968 |
| Matrix p factor | ϕ_1 | 0.5 | | | Walsh, 1981 |
| fracture p factor | ϕ_2 | 0.9 | | | Walsh, 1981 |
| Matrix permeability | k_1 | $10^{-10} \sim 10^{-14}$ | cm ² | sandstone | Freeze and Cherry, 1979 |
| Fracture permeability | k_2 | $10^{-7} \sim 10^{-11}$ | cm ² | metamorphic rocks | Freeze and Cherry, 1979 |
| Dynamic viscosity | μ | 0.012 | cP | oil | Craft and Hawkins, 1959 |
| | | 1.5 | cP | water | Craft and Hawkins, 1959 |
| Transfer coefficient | Γ | 60 | | parallelepiped | Warren and Root, 1963 |

tory techniques, in contrast to the physical parameters which are generally acquired via field measurements. For the determination of poromechanical parameters, more sophisticated macromechanical testing methods with fluid pressure coupling are usually required. As an initial approximation, Table 1 lists the values or the approximate ranges of general parameters which may be needed in the calculation. These parameters should be readjusted to suit individual situations. In particular, the mechanical parameters are basically determined from laboratory tests and should be adjusted to match in-situ magnitudes.

It should be realized that not all of the previously defined parameters are independent. The existence of some parameters is aimed at providing a definable and computational convenience. For example, using a similar approach as Nur and Byerlee (1971), the fluid pressure ratio factors ϕ_i , ($i=1,2$) in an overlapping matrix–fracture network may be defined as a function of the fluid, solid grain and skeleton bulk moduli, together with fracture compressibility:

$$\phi_1 = 1 - K \left(\frac{1}{K_f} + \frac{1}{K_g} \right) \quad (34)$$

for matrix, and:

$$\phi_2 = 1 - K \left(\frac{1}{K_f} + \frac{1}{K_n s^*} \right) \quad (35)$$

for fractures; where K is the bulk modulus of rock skeleton.

The matrix permeability k_1 may be associated with the matrix porosity via (Bear, 1972):

$$k_1 = \frac{n_1^3}{(1-n_1)^2} \frac{d_m^2}{180} \quad (36)$$

where d_m is the mean grain size or the hydraulic radius. Fracture permeability k_2 in the fracture-dominant porous rock mass may be related to the fracture spacing s^* by (Snow, 1968):

$$k_2 = \frac{b_f^3}{12s^*} \quad (37)$$

where b_f is the fracture aperture.

4. Dual-porosity behavior

The parameters used in an illustrative example are detailed in Table 2 for a fractured-porous reservoir of

Table 2
Parameters in an illustrative example

| Porosity n | | Factor ϕ | | Coefficient Radius | | | | |
|--------------|-----------|---------------|-----------|--------------------|----------|-------|----------|-------|
| Matrix | Fractures | Matrix | Fractures | ν | P_{Dw} | r_w | r_{De} | r_D |
| 0.2 | 0.02 | 0.5 | 0.9 | 0.25 | 1.0 | 0.1 m | 10,000 | 2.0 |

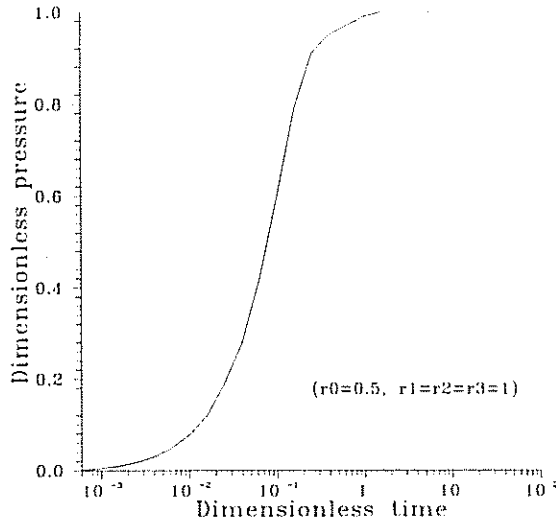


Fig. 2. Temporal pressure at $r_0 = 2$ under constant well pressure.

infinite extent. Assuming a constant pressure inner boundary and a no-flow boundary at infinity while considering the influence of fluid compressibility from the guest phase only, Fig. 2 shows the normalized temporal fluid pressure in the fractures when the ratio of $r_0 = k_1/k_2 = 0.5$, $r_1 = K_f/K_{ns}$, $r_2 = K_f/K_s$, $r_3 = K_f/E$ are all equal to one, and the elastic modulus equals 1 GPa. It is noted that the gradual pressure changes at early time demonstrates the substantial contribution from the intergranular matrix flow. The following dramatic fluid

pressure change at later time indicates dominated flow in more permeable fractures.

Another attempt is made to simulate a fractured-porous reservoir with a finite radius ($r_{Dc} = 10,000$). It is assumed that a constant fluid pressure prevails at the outer boundary, that a constant pumping rate is maintained at the wellbore, and that the reservoir is composed of equally-spaced fractured porous blocks. The parameters in the calculation are the same as those shown in Table 2, except that the dimensionless radius r_D equals 1.

Fig. 3 shows the dimensionless pressure-time relationship for a number of permeability ratios ($r_0 = k_1/k_2$). It is interesting to note that a decrease in matrix permeability results in a significantly delayed pressure drop in the fractures, representing the dominant impact of fracture flow.

For a fixed permeability ratio ($r = 0.01$) and compressibility ratio of fluid to rock elastic modulus ($r_3 = K_f/E = 1$), the pressure change is least sensitive to the change of compressibility ratios $r_1 = K_f/(K_{ns})$ and $r_2 = K_f/(K_s)$ at later times (Fig. 4). It appears that, for a constant fluid compressibility, a decrease in fracture compressibility leads to delayed pressure disturbance. The dual porosity behavior becomes observable at large r_1 . For larger r_1 , the fluid in the fractures is drained quickly, and the matrix storage supplies the fractures within a short period of time. Subsequently, fluid flow and fluid pressure between matrix and frac-

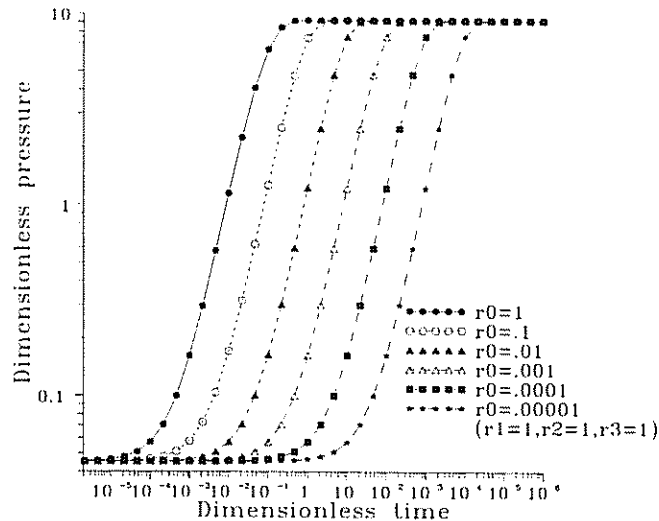


Fig. 3. Temporal pressure for various permeability ratios.

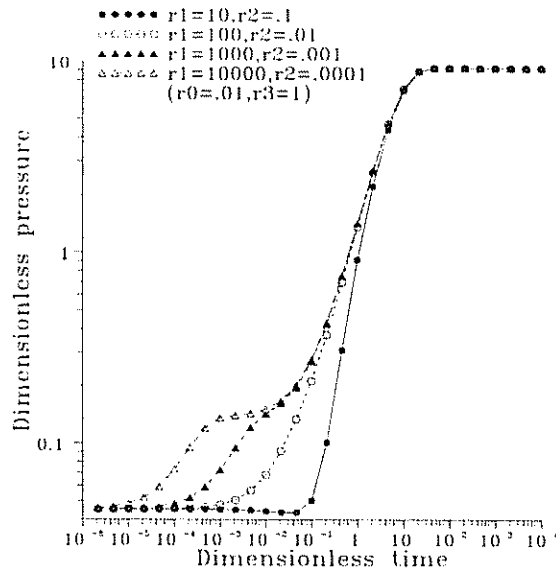


Fig. 4. Temporal pressure for various fracture and grain compressibilities (a).

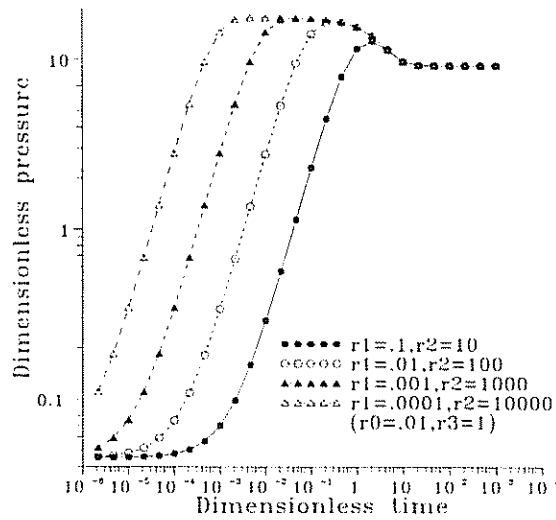


Fig. 5. Temporal pressure for various fracture and grain compressibilities (b).

tures are maintained in equilibrium within the system. For a fixed permeability ratio, r_0 , and compressibility ratio, r_3 , pressure profiles are sensitive to variation of the compressibility ratios r_1 and r_2 , as illustrated in Fig. 5. It is obvious that the pressure change is delayed as r_1 increases and r_2 decreases. This behavior resembles an equivalent homogeneous reservoir with soft frac-

tures and stiff solid grains. However, it is important to note that the depleting pressure magnitude at early periods appears greater than the reservoir pressure as depicted in Fig. 5. This poromechanical impact cannot be observed if a conventional flow model is used alone.

Dual-porosity behavior is exhibited if the elastic modulus of the rock mass is relatively large for fixed ratios of r_0 , r_1 and r_2 . The effect of the elastic constant of the rock mass diminishes when the ratio r_3 is smaller than 10^{-5} (Fig. 6). Although the duration is short at early dimensionless times, the pressure change is significant, depending on the magnitudes of r_3 . In addition, the period of pressure stabilization during the fluid transfer between matrix and fractures appears to be prolonged as a result of variation in r_3 . For a fixed Poisson ratio, the magnitude of rock elastic modulus represents the stiffness of the rock skeleton, which plays a critical role in the determination of the pressure profile. This effect is illustrated in Fig. 7, where the dual-porosity behavior is apparent only when the rock mass is relatively stiff, e.g. $r_3 = 0.01$. The poromechanical effect is obvious when r_3 falls in the range between 0.1 and 1000. Both dual-porosity phenomena and the poromechanical influence diminish when r_3 is equal or larger than 1000. Because large r_3 represents relatively soft rock masses, the dual-porosity behavior is least observable for soft media.

Assuming $r_D = 5$, $r_0 = 0.1$, $r_1 = r_2 = r_3 = 1$, and $2\pi h(k_1 + k_2) = q\mu/r_w$, the radial pressure and defor-

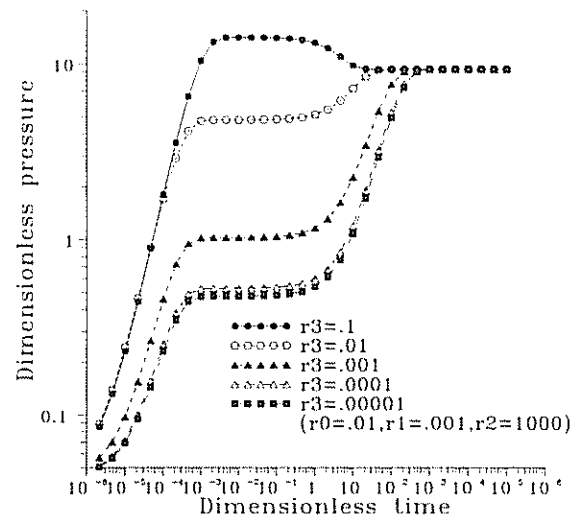


Fig. 6. Temporal pressure for various elastic constants (a).

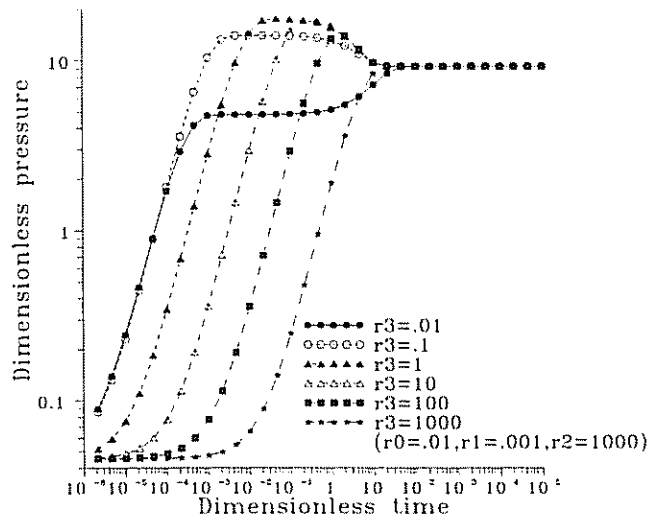


Fig. 7. Temporal pressure for various elastic constants (b).

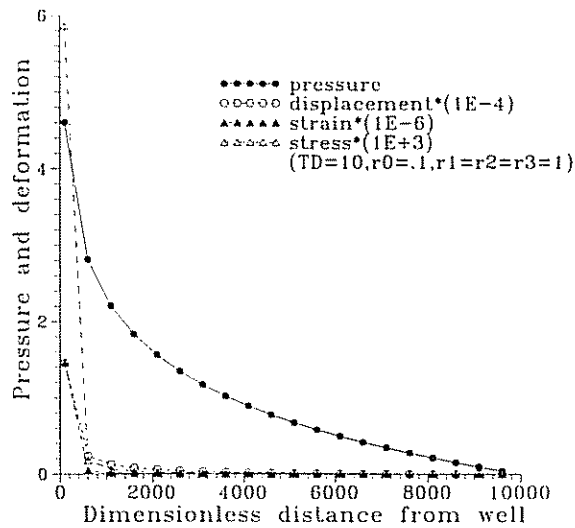


Fig. 8. Deformation and pressure profiles along radial distance.

mation profiles are illustrated in Fig. 8 when t_D equals 10. It is noted that unlike the uniform pressure decline from the well, both solid deformation and stress decline dramatically within a dimensionless distance of 600 from the well, signifying a significant local deformation effect as a result of petroleum production. This implies that the impact of poromechanical behavior should not be neglected within this region.

5. Conclusions

An analytical procedure has been presented to evaluate the poromechanical effects on the fluid pressure, the state of stress and the deformation near a well as a result of pumping in a fractured-porous rock mass. In comparison with conventional approaches to dual-porosity behavior, the present model provides a more reasonable description of the storage interaction

between matrix blocks and fractures, while simultaneously coupling displacements to the pore fluid response. As enabled by the characteristics of an infinite medium, the volumetric strain rate is partially decoupled from the impact of fluid pressure by applying a poromechanical potential. However, the coupling of flow with deformation is recovered by placing the fluid pressure gradient as a body force while maintaining the system in equilibrium. The poromechanical influence is most prominent near a producing well where the modifications of reservoir initial flow and deformation conditions are dramatic. Change in the flow system in the vicinity of a production well may, therefore, be misinterpreted without considering this important poromechanical factor. For a constant fluid compressibility, the dual-porosity behavior of the fractured-porous rock mass is identified at the early transient stage when fracture drainage leads to significant compression of the fractures. Dual-porosity behavior may not be observable if the rock skeleton is relatively soft, even if a significant disparity exists between fracture and grain compressibilities. However, the poromechanical influence is noticeable for soft rock masses, where the pressure magnitude at early time appears greater than the average reservoir pressure, a phenomenon not attainable using traditional diffusive flow models. Dual-porosity behavior is most obvious in reservoirs comprising a stiff rock mass with relatively small fracture compressibilities and large grain compressibilities. The decrease in the permeability ratio between matrix and fractures only results in the delay of temporal pressure magnitudes, while no dual-porosity behavior is apparent.

Acknowledgements

Support of National Science Foundation under contract EEC9209619 is greatly acknowledged.

Appendix A. Constant bottom hole pressure

During production, the bottom hole pressure is usually maintained at a constant level to prevent excessive separation of gas from oil. The boundary and initial conditions for an infinite reservoir with a constant bottom hole pressure and no flow at infinity are:

$$\begin{cases} P_{D1} = P_{D2}|_{r_D=1} = -P_{DW} \\ \frac{\partial P_{D1}}{\partial r_D} = \frac{\partial P_{D2}}{\partial r_D}|_{r_D \rightarrow \infty} = 0 \\ U_D|_{r_D \rightarrow \infty} = 0 \\ P_{D1} = P_{D2}|_{r_D=0} = 0 \end{cases} \quad (A1)$$

where P_{DW} is the dimensionless bottom hole pressure, which, for all practical purposes, is equal to or smaller than 1. For a linear system, the solution of Eqs. 32 and 33 can be expressed as:

$$P_{Di} = V_{Di} + P_{DW} \quad (i = 1, 2) \quad (A2)$$

The equations for the unknown V are:

$$\begin{aligned} \frac{\partial^2 V_{D1}}{\partial r_D^2} + \frac{1}{r_D} \frac{\partial V_{D1}}{\partial r_D} = \\ \omega_1 \frac{\partial V_{D1}}{\partial t_D} - \omega_2 \frac{\partial V_{D2}}{\partial t_D} + \lambda^* (V_{D1} - V_{D2}) \end{aligned} \quad (A3)$$

$$\begin{aligned} \frac{\partial^2 V_{D2}}{\partial r_D^2} + \frac{1}{r_D} \frac{\partial V_{D2}}{\partial r_D} = \\ \omega_3 \frac{\partial V_{D2}}{\partial t_D} - \omega_4 \frac{\partial V_{D1}}{\partial t_D} - \lambda^* R_k (V_{D1} - V_{D2}) \end{aligned} \quad (A4)$$

The boundary and initial conditions are:

$$\begin{cases} V_{D1} = V_{D2}|_{r_D=1} = 0 \\ V_{D1} = V_{D2}|_{r_D \rightarrow \infty} = 0 \\ V_{D1} = V_{D2}|_{r_D=0} = -P_{DW} \end{cases} \quad (A5)$$

Using the Hankel transform defined by:

$$\begin{aligned} \bar{V}_{Di}(\xi, t_D) = \int_1^\infty V_{Di}(r_D, t_D) \bar{\Psi}(\xi, r_D) r_D dr_D \\ (i = 1, 2) \end{aligned} \quad (A6)$$

where:

$$\begin{aligned} V_{Di}(r_D, t_D) = \int_1^\infty [J_0^2(\xi) + Y_0^2(\xi)]^{-1} \\ \bar{V}_{Di}(\xi, t_D) \bar{\Psi}(\xi, r_D) \xi d\xi \end{aligned} \quad (A7)$$

and ξ is an integral parameter; the Bessel function $\bar{\Psi}(\xi, r_D)$, which satisfies the boundary conditions shown in Eq. A5, is:

$$\bar{\Psi}(\xi, r_D) = Y_0(\xi)J_0(\xi r_D) - J_0(\xi)Y_0(\xi r_D) \quad (A8)$$

Solving Eqs. A3 and A4 using this Hankel transform gives:

$$-(\xi^2 + \lambda^*)\bar{V}_{D1} + \lambda^*\bar{V}_{D2} = \omega_1 \frac{d\bar{V}_{D1}}{dt_D} - \omega_2 \frac{d\bar{V}_{D2}}{dt_D} \quad (A9)$$

$$-(\xi^2 + \lambda^*R_k)\bar{V}_{D2} + \lambda^*R_k\bar{V}_{D1} = \omega_3 \frac{d\bar{V}_{D2}}{dt_D} - \omega_4 \frac{d\bar{V}_{D1}}{dt_D} \quad (A10)$$

For convenience, let us define:

$$\begin{cases} a_1 = (\xi^2 + \lambda^*) \\ a_2 = (\xi^2 + \lambda^*R_k) \\ b = \omega_1\omega_3 - \omega_2\omega_4 \\ c_{11} = (a_1\omega_3 - \lambda^*\omega_2R_k)b^{-1} \\ c_{12} = (a_2\omega_2 - \lambda^*\omega_3)b^{-1} \\ c_{21} = (a_1\omega_4 - \lambda^*\omega_1R_k)b^{-1} \\ c_{22} = (a_2\omega_1 - \lambda^*\omega_4)b^{-1} \end{cases} \quad (A11)$$

Eqs. A9 and A10 may be rewritten, after integration with respect to t_D , as:

$$\bar{V}_{D1} = \frac{c_{22}D}{d^*}e^{-c_{11}t_D} - \frac{c_{12}F}{d^*}e^{-c_{22}t_D} \quad (A12)$$

$$\bar{V}_{D2} = -\frac{c_{21}D}{d^*}e^{-c_{11}t_D} + \frac{c_{11}F}{d^*}e^{-c_{22}t_D} \quad (A13)$$

where:

$$d^* = c_{11}c_{22} - c_{12}c_{21} \quad (A14)$$

and D and F are determined from the initial condition. Substituting Eqs. A12 and A13 into A7, one obtains:

$$V_{D1} = \int_1^{\infty} \left(\frac{c_{22}}{d^*}De^{-c_{11}t_D} - \frac{c_{12}}{d^*}Fe^{-c_{22}t_D} \right) \bar{\Psi}^*(\xi, r_D) \xi d\xi \quad (A15)$$

$$V_{D2} = \int_1^{\infty} \left(-\frac{c_{21}}{d^*}De^{-c_{11}t_D} + \frac{c_{11}}{d^*}Fe^{-c_{22}t_D} \right) \bar{\Psi}^*(\xi, r_D) \xi d\xi \quad (A16)$$

where:

$$\bar{\Psi}^*(\xi, r_D) = \frac{\bar{\Psi}(\xi, r_D)}{J_0^2(\xi) + Y_0^2(\xi)} \quad (A17)$$

To satisfy the initial condition in Eq. A5, the following relationship between D and F can be obtained:

$$D = \frac{c_{11} + c_{12}F}{c_{21} + c_{22}} \quad (A18)$$

Finding explicit expressions for D and F is difficult due to the complication in solving the integrals in Eqs. A15 and A16. However, if flow between the matrix and the fractures is neglected on application of the initial conditions, or $\lambda^* = 0$, then the coefficients F and D may be determined from Eqs. A15 and A16; i.e.:

$$F = -P_{Dw} \left[\left(\frac{\omega_1\omega_3 - \omega_2\omega_4}{\omega_1 + \omega_4} \right) \int_1^{\infty} \bar{\Psi}^* \frac{d\xi}{\xi} \right]^{-1} \quad (A19)$$

$$D = -P_{Dw} \left[\omega_4 \left(\frac{\omega_1 - \omega_2 - \omega_3 + \omega_4}{\omega_2 + \omega_3} \right) \int_1^{\infty} \bar{\Psi}^* \frac{d\xi}{\xi} \right]^{-1} \quad (A20)$$

For $\lambda^* = 0$, Eqs. A15 and A16 may be rewritten as:

$$V_{D1} = F \int_1^{\infty} \left[\omega_1 \left(\frac{\omega_3 + \omega_2}{\omega_4 + \omega_1} \right) e^{-c_1 t_D} - \omega_2 e^{-c_2 t_D} \right] \bar{\Psi}^* \frac{d\xi}{\xi} \quad (A21)$$

$$V_{D2} = D \int_1^{\infty} \omega_4 \left[-e^{-c_1 t_D} + \left(\frac{\omega_1 + \omega_4}{\omega_2 + \omega_3} \right) e^{-c_2 t_D} \right] \bar{\Psi}^* \frac{d\xi}{\xi} \quad (A22)$$

where F and D may be calculated from Eqs. A19 and A20; and:

$$c_1^* = \frac{\omega_3}{\omega_1\omega_3 - \omega_2\omega_4} \quad (A23)$$

$$c_2^* = \frac{\omega_1}{\omega_1\omega_3 - \omega_2\omega_4} \quad (A24)$$

Alternatively, the general expressions for D and F may be determined from Eqs. A15 and A16 using an iterative solution procedure with direct elimination through supplying D or F with initial values. Fluid pressures can then be determined from Eqs. A2, A15 and A16:

$$P_{D1} = \int_1^{\infty} \left[\frac{c_{22}}{d^*}De^{-c_{11}t_D} - \frac{c_{12}}{d^*}Fe^{-c_{22}t_D} \right] \bar{\Psi}^*(\xi, r_D) \xi d\xi + P_{Dw} \quad (A25)$$

$$P_{D2} = \int_1^{\infty} \left[-\frac{c_{21}}{d^*}De^{-c_{11}t_D} + \frac{c_{11}}{d^*}Fe^{-c_{22}t_D} \right] \bar{\Psi}^*(\xi, r_D) \xi d\xi + P_{Dw} \quad (A26)$$

The solutions of Eqs. A25 and A26 may be obtained using a numerical integration technique. In the present analysis, an adaptive Simpson's integration method was chosen, whereby the entire interval is continuously subdivided into subintervals of variable lengths until a prescribed accuracy is achieved. The outer boundary is theoretically at infinity, although it is practically determined by the vanishing magnitude of pressure P_D . From Eqs. A25 and A26, it is readily verified that, as r_D approaches infinity, fluid pressures in the matrix blocks and in the fractures approach a constant value P_{Dw} .

It is understood that P_{D1} and P_{D2} are now known functions. Eq. 31 may be integrated to yield:

$$U_D = \frac{1}{r_D} \left[-\beta^* \int_1^{\eta} (\phi_1 P_{D1} + \phi_2 P_{D2}) r_D dr_D + g(t) \right] \quad (\text{A27})$$

where $g(t)$ can be determined by satisfying the boundary condition (A1) as:

$$g(t) = \beta^* \int_1^{\infty} (\phi_1 P_{D1} + \phi_2 P_{D2}) r_D dr_D \quad (\text{A28})$$

Dimensionless strains may be deduced from Eqs. 17, 18 and 31 as:

$$\begin{aligned} \epsilon_{Drr} &= \frac{\partial U_D}{\partial r_D} \\ &= \beta^* \left\{ \frac{1}{r_D^2} \left[\int_1^{\eta} (\phi_1 P_{D1} + \phi_2 P_{D2}) r_D dr_D - \right. \right. \end{aligned} \quad (\text{A29})$$

$$\begin{aligned} &\left. \int_1^{\infty} (\phi_1 P_{D1} + \phi_2 P_{D2}) r_D dr_D \right] - (\phi_1 P_{D1} + \phi_2 P_{D2}) \Big\} \\ \epsilon_{D\theta\theta} &= \frac{U_D}{r_D} = \frac{\beta^*}{r_D^2} \\ &\left[- \int_1^{\eta} (\phi_1 P_{D1} + \phi_2 P_{D2}) r_D dr_D \right. \quad (\text{A30}) \\ &\left. + \int_1^{\infty} (\phi_1 P_{D1} + \phi_2 P_{D2}) r_D dr_D \right] \end{aligned}$$

Dimensionless stresses are deduced from Eqs. 19 and 20; i.e.:

$$\begin{aligned} \sigma_{Drr} &= \beta^{-1} \epsilon_{Drr} + \lambda \epsilon_{D\theta\theta} \\ &\quad + \alpha_1 (\phi_1 P_{D1} + \phi_2 P_{D2}) \end{aligned} \quad (\text{A31})$$

where:

$$\alpha_1 = \beta^* \beta^{-1} \quad (\text{A32})$$

Or written in an explicit form:

$$\begin{aligned} \sigma_{Drr} &= \frac{\beta^* (\beta^{-1} - \lambda)}{r_D^2} \\ &\left[\int_1^{\eta} (\phi_1 P_{D1} + \phi_2 P_{D2}) r_D dr_D \right. \quad (\text{A33}) \\ &\left. - \int_1^{\infty} (\phi_1 P_{D1} + \phi_2 P_{D2}) r_D dr_D \right] \end{aligned}$$

$$\begin{aligned} \sigma_{D\theta\theta} &= \beta^{-1} \epsilon_{D\theta\theta} + \lambda \epsilon_{Drr} + \alpha_1 (\phi_1 P_{D1} + \phi_2 P_{D2}) \\ &= \frac{\beta^*}{r_D^2} (\lambda - \beta^{-1}) \left[\int_1^{\eta} (\phi_1 P_{D1} + \phi_2 P_{D2}) r_D dr_D \right. \\ &\quad \left. - \int_1^{\infty} (\phi_1 P_{D1} + \phi_2 P_{D2}) r_D dr_D \right] \\ &\quad + (\alpha_1 - \lambda \beta^*) (\phi_1 P_{D1} + \phi_2 P_{D2}) \end{aligned} \quad (\text{A34})$$

It is seen from these expressions that the radial displacements, strains and stresses disappear at infinity.

Appendix B. Constant pumping rate

Reservoir pressure measurements are usually recorded in the production well while maintaining a constant flow rate, which is also a normal operation requirement in well testing. In petroleum engineering, reservoirs with a finite boundary are more frequently encountered than those with an infinite boundary as discussed for the case of constant bottom hole pressure. For a finite reservoir, the decoupling of the volumetric strain from the fluid pressure is valid as long as the reservoir outer boundary is sufficiently large that the

effect of the outer boundary on the reservoir fluid pressure change is negligible.

The boundary and initial conditions for a finite reservoir with a constant outer boundary and a constant pumping rate (assuming average flow between fractures and matrix at the well) are:

$$\begin{cases} \frac{\partial P_{D1}}{\partial r_D} = \frac{\partial P_{D2}}{\partial r_D} \Big|_{r_D=1} = -1 \\ P_{D1} = P_{D2} \Big|_{r_D=r_{Dc}} = 0 \\ P_{D1} = P_{D2} \Big|_{r_D=0} = 0 \\ U_D \Big|_{r_D=r_{Dc}} = 0 \end{cases} \quad (B1)$$

Similar to Eq. A2, the solution of the equations governing flow may be expressed as:

$$P_{Di} = V_{Di} + \ln(r_{Dc}) - \ln(r_D) \quad (i = 1, 2) \quad (B2)$$

The governing equations for V_{Di} possess an identical form to Eqs. A3 and A4. The boundary and initial conditions are:

$$\begin{cases} \frac{\partial V_{D1}}{\partial r_D} = \frac{\partial V_{D2}}{\partial r_D} \Big|_{r_D=1} = 0 \\ V_{D1} = V_{D2} \Big|_{r_D=r_{Dc}} = 0 \\ V_{D1} = V_{D2} \Big|_{r_D=0} = -[\ln(r_{Dc}) - \ln(r_D)] \end{cases} \quad (B3)$$

The boundary value problems can be solved using a general finite Hankel transform defined as:

$$\bar{V}_{Di}(j, t_D) = \int_1^{r_{Dc}} V_{Di}(r_D, t_D) \Phi_j(r_D) r_D dr_D \quad (i = 1, 2) \quad (B4)$$

where:

$$V_{Di}(r_D, t_D) = \sum_{j=1}^{\infty} G_j \bar{V}_{Di}(j, t_D) \Phi_j(r_D) \quad (B5)$$

and G_j is a coefficient to be determined from the initial conditions. $\Phi_j(r_D)$, which satisfies the boundary conditions in Eq. B3, may be expressed as:

$$\Phi_j(r_D) = Y_0(\xi_j r_{Dc}) J_0(\xi_j r_D) - J_0(\xi_j r_{Dc}) Y_0(\xi_j r_D) \quad (B6)$$

and can be obtained by solving the eigenvalue problem. Terms ξ_j are the roots of the following equation:

$$J_1(\xi_j) Y_0(\xi_j r_{Dc}) - J_0(\xi_j r_{Dc}) Y_1(\xi_j) = 0 \quad (B7)$$

Applying the finite Hankel transform, governing equations that are identical to Eqs. A9 and A10 can be obtained except that now ξ_j replaces ξ . Following the procedure described previously, yields:

$$V_{D1} = \sum_{j=1}^{\infty} \Phi_j(r_D) (c_{22} D_j e^{-c_{11} t_D} - c_{12} F_j e^{-c_{22} t_D}) \quad (B8)$$

$$V_{D2} = \sum_{j=1}^{\infty} \Phi_j(r_D) (-c_{21} D_j e^{-c_{11} t_D} + c_{11} F_j e^{-c_{22} t_D}) \quad (B9)$$

where D_j and F_j are related to G_j ; all other coefficients have been previously defined where ξ_j replaces ξ . Using orthogonal properties, D_j and F_j are obtained to satisfy the initial condition in Eq. B3. Hence:

$$D_j = -(c_{11} + c_{12}) \quad (B10)$$

$$\begin{aligned} & [\ln(r_{Dc}) - \ln(r_D)] \pi (d^*)^{-1} \\ F_j = -(c_{21} + c_{22}) & \quad (B11) \\ & [\ln(r_{Dc}) - \ln(r_D)] \pi (d^*)^{-1} \end{aligned}$$

The governing equations for fluid pressure may finally be written as:

$$P_{D1} = \sum_{j=1}^{\infty} \Phi_j(r_D) (c_{22} D_j e^{-c_{11} t_D} - c_{12} F_j e^{-c_{22} t_D}) + \ln(r_{Dc}) - \ln(r_D) \quad (B12)$$

$$P_{D2} = \sum_{j=1}^{\infty} \Phi_j(r_D) (-c_{21} D_j e^{-c_{11} t_D} + c_{11} F_j e^{-c_{22} t_D}) + \ln(r_{Dc}) - \ln(r_D) \quad (B13)$$

After obtaining P_{D1} and P_{D2} from Eqs. B12 and B13, the dimensionless displacement U_D is determined from Eq. A27, which satisfies the boundary conditions given by Eq. B1:

$$U_D = \frac{\beta^*}{r_D} \left\{ \frac{(\phi_1 + \phi_2)}{2} \left[\frac{1}{2} (r_{Dc}^2 - r_D^2) + r_D^2 [\ln(r_D) - \ln(r_{Dc})] \right] \right\}$$

$$\sum_{j=1}^{\infty} \frac{2H}{\pi \xi_j^2} \left[\frac{\ln(r_{Dc})}{J_0(\xi_j)} [J_0(\xi_j r_{Dc}) - J_0(\xi_j r_D)] + \ln(r_{Dc}) - \ln(r_D) \right] \quad (B14)$$

where:

$$H = \frac{-\pi}{d^*} \left[(c_{11} + c_{12}) (\phi_1 c_{22} - \phi_2 c_{21}) e^{-c_{11} d} + (c_{21} + c_{22}) (\phi_2 c_{11} - \phi_1 c_{12}) e^{-c_{22} d} \right] \quad (B15)$$

The derivative of the displacement may be derived from Eq. 31 as an alternative to direct differentiation from Eq. B15.

$$\frac{\partial U_D}{\partial r_D} = - \left[\frac{U_D}{r_D} + \beta^* (\phi_1 P_{D1} + \phi_2 P_{D2}) \right] \quad (B16)$$

Strains and stresses can be readily obtained following a procedure similar to that used for Eqs. A29, A30, A31 and A34.

References

- Barenblatt, G.I., Zheltov, I.P. and Kochina, N., 1960. Basic concepts in the theory of seepage of homogeneous liquids in fissured rocks. *Prikl. Mat. Mekh.*, 24(5): 852–864.
- Barenblatt, G.I., Entov, V.M. and Ryzhik, V.M., 1990. *Theory of Fluid Flows through Natural Rocks*. Kluwer Academic Publisher, Dordrecht, 395 pp.
- Bai, M., Elsworth, D. and Roegiers, J.-C., 1993. Multi-porosity/multi-permeability approach to the simulation of naturally fractured reservoirs. *Water Resour. Res.*, 29(6): 1621–1633.
- Bai, M., Ma, Q. and Roegiers, J.-C., 1994. A nonlinear dual-porosity model. *Appl. Math. Modelling*, 18: 602–610.
- Bai, M. and Meng, F., 1994. Study of naturally fractured reservoirs using three-dimensional finite elements. *RMRC Rep.*, 9419.
- Bai, M. and Roegiers, J.-C., 1994. On the correlation of nonlinear flow and linear transport with application to dual-porosity modeling. *J. Pet. Sci. Eng.*, 11: 63–72.
- Bai, M. and Roegiers, J.-C., 1995. Modeling of heat flow and solute transport in fractured rock masses. *Proc. 8th Int. Congress Rock Mechanics*, Japan.
- Bear, J., 1972. *Dynamics of Fluids in Porous Media*. Elsevier, New York, N.Y., 764 pp.
- Biot, M.A., 1941. General theory of three-dimensional consolidation. *J. Appl. Phys.*, 12: 155–164.
- Biot, M.A., 1956. Thermoelasticity and irreversible thermodynamics. *J. Appl. Phys.*, 27: 240–253.
- Cleary, M.P., 1977. Fundamental solutions for a fluid-saturated porous solid. *Int. J. Solids Struct.*, 13: 785–808.
- Craft, B.C. and Hawkins, M.F., 1959. *Applied Petroleum Reservoir Engineering*. Prentice-Hall, Englewood Cliff, N.J., 437 pp.
- Cryer, C.W., 1962. A comparison of the three-dimensional consolidation theories of Biot and Terzaghi. *Q. J. Mech. Appl. Math.*, 16: 401–412.
- Curran, J. and Carvalho, J.L., 1987. A displacement discontinuity model for fluid-saturated porous media. *Proc. 6th Int. Congr. Rock Mechanics*, Montreal, Canada. Balkema, Rotterdam, pp. 73–78.
- Freeze, R.A. and Cherry, J.A., 1979. *Groundwater*. Prentice-Hall, Englewood Cliff, N.J., 604 pp.
- Goodier, J.N., 1936. The thermal stresses in a strip. *Physics*, 7: 156.
- Iwai, K., 1976. *Fundamental studies of fluid flow through a single fracture*. Ph.D. diss., Univ. California, Berkeley, Calif., 208 pp.
- Jumikis, A.R., 1983. *Rock Mechanics*, 2nd ed. Trans. Tech. Publ., Houston, Tex., 613 pp.
- Melan, E., 1940. Der Spannungszustand der durch eine Einzelkraft im innern beanspruchten Halbscheibe. *Angew. Math. Mech.*, 12: 343–346, 1932 (Correction: *Z. Angew. Math. Mech.*, 20: 368).
- Moench, A.F., 1984. Double-porosity models for a fissured groundwater reservoir with fracture skin. *Water Resour. Res.*, 20: 831–846.
- Nur, A. and Byerlee, J.D., 1971. An exact effective stress law for elastic deformation of rock with fluids. *J. Geophys. Res.*, 76(26): 6414–6419.
- Raghavan, R., 1977. Pressure behavior of wells intercepting fractures. *Invitational Well-Testing Symp.*, Lawrence Berkeley Lab., Calif.
- Rice, J.R. and Cleary, M.P., 1976. Some basic stress-diffusion solutions for fluid saturated elastic porous media with compressible constituents. *Rev. Geophys. Space Phys.*, 14: 227–241.
- Rosso, R.S., 1976. A comparison of joint stiffness measurements in direct shear, triaxial compression, and in situ. *Int. Rock Mech. Min. Sci. Geomech. Abstr.*, 13: 167–172.
- Segall, P., 1985. Stress and subsidence resulting from subsurface fluid withdrawal in the epicentral region of the 1983 Coalinga earthquake. *J. Geophys. Res.*, B8: 6801–6816.
- Snow, D.T., 1968. Rock fracture spacings, openings, and porosities. *J. Soil Mech. Found. Div., Proc. ASCE*, 94: 73–91.
- Streltsova-Adams, T.D., 1978. Well hydraulics in heterogeneous aquifer formations. *Adv. Hydrosci.*, 11: 357–423.
- Terzaghi, K.V., 1923. Die Berechnung der Durchlässigkeit der Tonen aus dem Verlauf der hydrodynamischen Spannungsercheinungen. *Sitzungsber. Akad. Wiss. Wien Math Naturwiss., Kl. Abt. 2A*, 132: 105.
- Walsh, J.B., 1981. Effect of pore pressure and confining pressure on fracture permeability. *Int. J. Rock Mech. Min. Sci. Geomech. Abstr.*, 18(3): 429–435.
- Warren, J.E. and Root, P.J., 1963. The behavior of naturally fractured reservoirs. *J. Soc. Pet. Eng.*, 3: 245–255.
- Wilson, R.K. and Aifantis, E.C., 1982. On the theory of consolidation with double porosity. *Int. J. Eng. Sci.*, 20(9): 1009–1035.